Research Article

Image Watermark Based on Extended Shearlet and Insertion Using the Largest Information Entropy on Horizontal Cone

Zhao Jian,[1] Sun Meiling,[1] Jia Jian,[2] Huang Luxi,[1] Han Fan,[1] and Liu Shan[1]

[1]*School of Information Science and Technology, Northwest University, Xi'an 710069, China*
[2]*School of Mathematical Science, Northwest University, Xi'an 710069, China*

Correspondence should be addressed to Zhao Jian; zjctec@nwu.edu.cn

Extended discrete shearlet provides a directional multiresolution decomposition. It has been mathematically shown that extended discrete shearlet is a more efficient representation for the signals containing distributed discontinuities such as edges, compared to discrete wavelet. Multiresolution analyses such as curvelet and ridgelet share similar properties, yet their directional representations are significantly different from that of extended discrete shearlet. Taking advantage of the unique properties of directional representation of extended discrete shearlet, we develop an image watermark algorithm based on the largest information entropy. In proposed algorithm, firstly, 1-level extended discrete shearlet transform decomposes the test image into directional components on horizontal cone; each directional component reflects directional features and textured features differently. Next, the directional component whose information entropy is the highest is selected to carry watermark. Compared with related algorithms based on DWT and DCT, the proposed algorithm tends to obtain preferable invisibility when it is robust against common attacks.

1. Introduction

Image watermark is one of the most active and challenging subjects in the information hiding research because it is an efficient solution to protect the copyright of the digital media. Wavelets have been widely applied in image watermark owning to their perfect performance for piecewise smooth signals in one dimension [1, 2].

However, wavelets are not actually optimal representation for signals in two dimensions or higher dimensions such as images [3–7]. In fact, wavelets not only fail to preserve the detailed features but they also fail to capture the directional features [3, 7]. With the development of multiresolution analysis, various multiresolution methods have been proposed to overcome this limitation of wavelets, and it has been experimentally proved that these multiresolution methods perform well in image watermark [4, 5, 8]. Among various multiresolution methods, discrete shearlet [6, 9] is a relatively new multiresolution method, which has drawn considerable attention and has been applied in some fields of image processing such as image denoising, image approximations,

and image inpainting for its superior performance in dealing with signals in high dimensions [6, 9–11]. Extended discrete shearlet [9, 11] is derived from discrete shearlet transform. It is based on a simple but rigorous mathematical framework which is composed of directional orthonormal bases; each orthonormal base exhibits high directional sensitivity and is highly anisotropic. The extended discrete shearlet transform attempts to obtain a sparse image representation which contains more directional information and preserves more detailed information than discrete wavelet.

Taking advantage of these unique properties of extended discrete shearlet, we develop an image watermark algorithm based on extended discrete shearlet transform and the largest information entropy [12, 13]. In proposed algorithm, by using extended discrete shearlet transform, an image is composed into directional components on the horizontal cone; each directional component is transformed into a set of shearlet coefficients. The watermark is embedded into the largest coefficients of the directional component whose information entropy is the highest. The proposed algorithm is compared with DCT-based algorithm and DWT-based algorithm.

2. Correlation with Basic Theory

2.1. Correlation with Shearlet Transform. A 2D affine system with composite dilations [6, 9, 14] is described by

$$\mathrm{SH}\left(\psi\right) = \left\{ \psi_{a,s,t}\left(x\right) = a^{-3/4}\psi\left(A_a^{-1}B_s^{-1}\left(x-t\right)\right) \right.$$

$$= a^{-3/4}\psi\left(\left(\begin{pmatrix} \dfrac{1}{a} & -\dfrac{s}{a} \\ 0 & \dfrac{1}{\sqrt{a}} \end{pmatrix} x - t\right)\right), \ a > 0, \ s \in R, \ t \quad (1)$$

$$\left. \in R^2 \right\},$$

where the parabolic scaling matrices $A_a = (a, 0; 0, \sqrt{a})$ ($a > 0$) are associated with scale transform and the shear matrices $B_s = (1, s; 0, 1)$ are related to area-preserving geometrical transform. The generating function ψ is chosen like a tensor product by

$$\widehat{\psi}\left(\xi\right) = \widehat{\psi}\left(\xi_1, \xi_2\right) = \widehat{\psi}_1\left(\xi_1\right)\widehat{\psi}_2\left(\frac{\xi_2}{\xi_1}\right), \quad (2)$$

where ψ_1 is continuous wavelet which is supported with supp $\widehat{\psi}_1 \subset [-2, -1/2] \cup [1/2, 2]$ and ψ_2 is a bump function with certain weak additional properties and is supported with supp $\widehat{\psi}_2 \subset [-1, 1]$.

The associated continuous shearlet transform [6, 9–11, 14] is defined by

$$\mathrm{SH}_f\left(a, s, t\right) = \left\langle f, \psi_{a,s,t} \right\rangle. \quad (3)$$

The shearlet transform is a function associated with a, s, and t, whereas wavelet transform is a function which is merely associated with a and t. The main idea of the shear parameter s is to capture directional features, such as orientations of curves [6, 9, 11]. As a consequence, the shearlet is able to capture directional information. Figure 1 illustrates the ability of capturing directions of the shearlet transform.

2.2. Correlation with Discrete Shearlet Transform. By sampling SH(ψ) on an appropriate discrete set of a, s, and t, a discrete shearlet transform is obtained [6, 9, 10, 14]. The discrete shearlet transform is described by

$$\left\{ \psi_{j,l,k}^{(d)}\left(x\right) = \left|\det A_d\right|^{j/2}\psi\left(B_d^l A_d^j x - k\right) : j \geq 0, \right.$$

$$\left. -\left\lceil 2^{j/2} \right\rceil \leq l \leq \left\lceil 2^{j/2} \right\rceil, \ k \in Z^2, \ d = 0, 1 \right\}, \quad (4)$$

where $A_0 = (4, 0; 0, 2)$, $A_1 = (2, 0; 0, 4)$, $B_0 = (1, 0; 1, 1)$, and $B_1 = (1, 1; 0, 1)$. If $\psi_{j,l,k}^{(d)}$ satisfy the property

$$\sum_{j,l,k} \left|\left\langle f, \psi_{j,l,k}^{(d)} \right\rangle\right|^2 = \|f\|^2, \quad (5)$$

the discrete shearlet transform forms a tight frame for $L^2(R)$.

For any $\xi = (\xi_1, \xi_2) \in \widehat{R}^2$, $\xi_1 \neq 0$, suppose

$$\sum_{j \geq 0} \left|\widehat{\psi}_1\left(2^{-2j}\omega\right)\right|^2 = 1 \quad \text{for } |\omega| \geq \frac{1}{8};$$

$$\sum_{l=-2^j}^{2^j} \left|\widehat{\psi}_2\left(2^j\omega - l\right)\right|^2 = 1 \quad \text{for } |\omega| \leq 1. \quad (6)$$

Specifically, define

$$\widehat{\psi}^{(0)}\left(\omega\right) = \widehat{\psi}^{(0)}\left(\omega_1, \omega_2\right) = \widehat{\psi}_1\left(\omega_1\right)\widehat{\psi}_2\left(\frac{\omega_2}{\omega_1}\right),$$

$$\widehat{\psi}^{(1)}\left(\omega\right) = \widehat{\psi}^{(1)}\left(\omega_1, \omega_2\right) = \widehat{\psi}_1\left(\omega_2\right)\widehat{\psi}_2\left(\frac{\omega_1}{\omega_2}\right), \quad (7)$$

where ψ_1 is a discrete wavelet function with supp $\widehat{\psi}_1 \subset [-1/2, -1/16] \cup [1/16, 1/2]$ and ψ_2 is a bump function with supp $\widehat{\psi}_2 \subset [-1, 1]$. From the supporting condition of $\widehat{\psi}_1$ and $\widehat{\psi}_2$, $\psi_{j,l,k}$ in frequency domain is supported with

$$\mathrm{supp}\,\widehat{\psi}_{j,l,k}^{(0)} \subset \left\{ (\omega_1, \omega_2) : \omega_1 \in \left[-2^{2j-1}, -2^{2j-4}\right] \right.$$

$$\left. \cup \left[2^{2j-4}, 2^{2j-1}\right], \ \left|l2^{-j} + \frac{\omega_2}{\omega_1}\right| \leq 2^{-j} \right\}. \quad (8)$$

Equation (8) implies that each element $\widehat{\psi}_{j,l,k}$ is supported on a pair of trapezoids, each of which is contained in a box of approximate size $2^{2j} \times 2^j$ and oriented along line of slope $-l2^{-j}$ [6, 9, 10, 14].

2.3. Correlation with Extended Discrete Shearlet. Extended discrete shearlet [6, 11] is obtained by directly extending discrete shearlet. Yet its framework is slightly different from that of the discrete shearlet. Framework of the extended discrete shearlet is composed of directional orthonormal bases; each orthonormal basis provides anisotropic window functions elongated along the direction determined by shear matrix. In addition, the extended discrete shearlet framework uses a MRA approach to compute shearlet coefficients and uses an iterative method to approximate the inverse. Based on this construction, a given image is explicitly decomposed into variously directional components for different cones when extended discrete shearlet is associated with different shear matrices and direction numbers; each directional component reflects directional features and textured features differently (see Figure 2); besides, a stable reconstruction of a given image is obtained.

Actually, the extended discrete shearlet framework exhibits highly directional sensitivity; and, furthermore, the extended discrete shearlet framework is optimally sparse representation and is well localized in both the spatial and the frequency domains. Based on these properties, the extended discrete shearlet can be considered as an appropriate transform for image watermark.
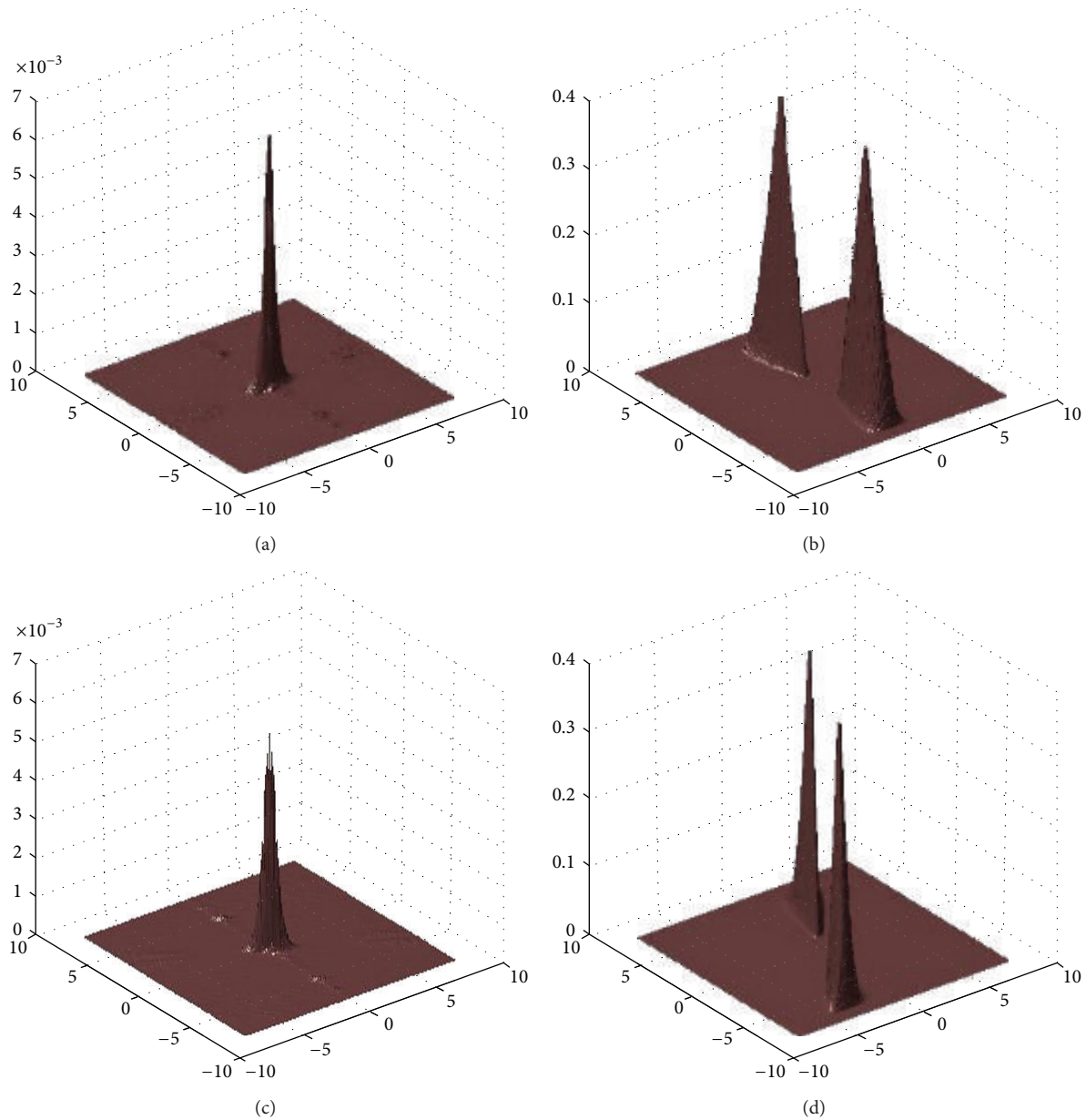
Figure 1: (a) $\psi_{a,s,t}$ in the time domain for $a = 0.3$, $s = 0$, and $t = 0$. (b) $\psi_{a,s,t}$ in the frequency domain for $a = 0.3$, $s = 0$, and $t = 0$. (c) $\psi_{a,s,t}$ in the time domain for $a = 0.3$, $s = -0.5$, and $t = 0$. (d) $\psi_{a,s,t}$ in frequency domain for $a = 0.3$, $s = -0.5$, and $t = 0$.

3. A Novel Watermark Algorithm Based on Extended Discrete Shearlet

The most important issue in extended discrete shearlet-based watermark algorithm is how to choose the watermark embedding location or the effective coefficients to be embedded, since the choice of watermark embedding location has an effect on both invisibility and robustness of watermark algorithm to some extent [1, 2, 4, 5, 8]. In this section, a novel algorithm for image watermark is proposed, which is based on combining the analysis of extended discrete shearlet coefficients [6, 11] and the basic theory of the largest information entropy to search the watermark embedding location for different images.

3.1. Analysis of Extended Discrete Shearlet Coefficients.
After 1-level extended discrete shearlet decomposition associated with shear matrix B_0 and direction numbers m, the test image of size $N \times N$ is decomposed into m directional components on horizontal cone (see Figure 2(b)); each of directional components is transformed into a set of shearlet coefficients.

Each directional component reflects directional features and preserved textured features differently; therefore, the occurring probabilities of different pixel values in each directional component are different from those of all others and the probability distribution of each directional component's information is different from that of all others in confusion degree. The higher information entropy [12, 13] of the directional component is, the more uncertain occurring

Original image

(a)

Shearlet coefficients for horizontal cone   Shearlet coefficients for horizontal cone

(b)

Shearlet coefficients for vertical cone   Shearlet coefficients for vertical cone

(c)
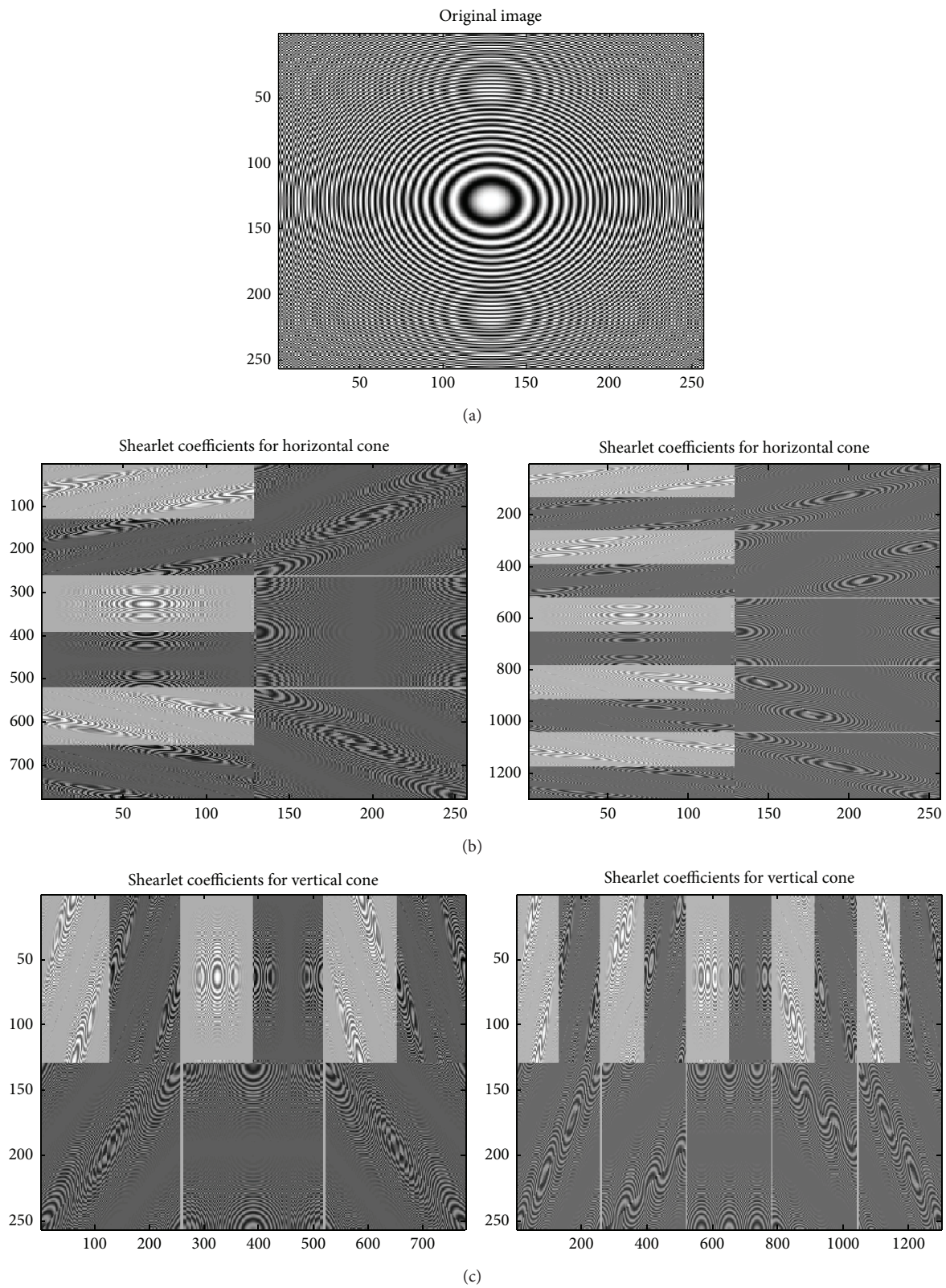
FIGURE 2: The extended discrete shearlet transform results corresponding to different directions and shear matrices.

probabilities of its different pixel values are, and probability distribution of its information is more disordered and more chaotic; that means it can hide more watermark bits. Based on this analysis, the directional component whose information entropy is the largest is selected to carry watermark. The information entropy of the lth directional component on horizontal cone is computed as follows:

(1) Mark pixel values of the lth directional component by $(X_1^l, X_2^l, \ldots, X_{N*N}^l)$.

(2) Count occurring probability $(p_1^l, p_2^l, \ldots, p_j^l, \ldots, p_K^l)$ of different pixel values of the lth directional component; here K is the total number of different pixel values.

(3) Calculate the information entropy of the lth directional component by

$$S^l = -\sum_{j=1}^{K} p_j^l \log_2\left(p_j^l\right), \tag{9}$$

where l $(l = 1, \ldots, m)$.

Generally, watermark insertion is realized by modifying some special values of pixels or transforming domain coefficients [1, 2, 4, 5]. Here watermark insertion is realized by modifying the largest $n \times n$ coefficients of selected directional component in extended discrete shearlet domain.

3.2. Watermark Insertion Using the Largest Information Entropy. For an image w used as watermark, in order to uniformly and randomly spread bits over the host image, it needs to be transformed into a binary image by

$$ww(i, j) = \begin{cases} -1 & \text{if } w(i, j) > \text{Tr} \\ 1 & \text{else}, \end{cases} \quad 1 \le i, j \le n. \tag{10}$$

Here threshold Tr is selected by *OSTA* method. After processing the watermark image w, a binary image ww is obtained and then reshaped to binary sequence wm with length $n \times n$.

According to the above analysis in Section 3.1, the directional component, whose information entropy is the highest, can hide more watermark bits and is selected to carry watermark. To obtain directional components on horizontal cone, a l-level extended discrete shearlet decomposition is applied to test image I with size $N \times N$, which is associated with shear matrix B_0 and direction numbers m. Then, to find out the directional component whose information entropy is the highest, information entropy of each directional component on horizontal cone is computed by (9).

Here we suppose the pth $(1 \le p \le m)$ directional component's information entropy is the highest. Then the binary sequence wm is embedded into the largest $n \times n$ coefficients of the pth directional component by

$$y^{(p)}(i, j)$$

$$= \begin{cases} x^{(p)}(i, j)(1 + a \times b(k)), & \text{if } x^{(p)}(i, j) \ge T \\ x^{(p)}(i, j), & \text{else}, \end{cases} \tag{11}$$

where $1 \le k \le n \times n$, a is used to control embedding strength, and T is the threshold.

Finally, the watermarked image I_w is obtained after 1-level extended inverse discrete shearlet transform by using these modified shearlet coefficients.

3.3. Watermark Extraction. The watermark can be extracted correctly from the watermarked image without original test image. The extracting process is as follows, which is mirroring embedding process.

To extract embedded watermark bits from the watermarked image, 1-level extended discrete shearlet decomposition is firstly applied to the watermarked image, where the shear matrix is selected as B_0 and the number of direction is n; then shearlet coefficients of every directional component on horizontal cone are obtained.

Then, the watermarked coefficients are found out according to watermark size and the location key of embedding watermark. The extracted watermark bits are recovered into a sequence $\vec{m}$ by

$$m(t) = \frac{\left(x_{ij}'^{(p)} - x_{(i,j)}^{(p)}\right)}{a \times x_{(i,j)}^{(p)}}, \quad \text{when } x_{ij}^{(p)} \ge T, \tag{12}$$

where $1 \le i, j \le N$, $1 \le t \le n \times n$, and T is the threshold.

Finally, the extracted watermark ww' is recovered by reshaping $\vec{m}$.

4. Experimental Results

4.1. Invisibility of Watermark. Invisibility is an evaluative measure of perceptual quality of the watermarked image. In a satisfactory image watermark algorithm, watermark should not cause much degradation of perceptual quality of the watermarked image. In the proposed algorithm, a 64×64 watermark image is embedded into different test images ("Lena," "Boat," and "Barbara" with 512×512) to test invisibility, where the number of directions is 9 and the embedding strength is 0.1.

As shown in Table 1, there are not much visual differences between original test images and their corresponding watermarked images. In addition, the PSNR value of each watermarked image is above 53 dB, and NC value of corresponding extracted watermark image is above 0.98. The extracted watermarks are all easily distinguishable. Whether from a subjective view or from the objective view, the proposed algorithm has preferable invisibility.

Furthermore, by analyzing the absolute difference between the test image and the watermarked image, it is not difficult to find that the watermark tends to spread on these regions with strong edges and extreme brightness. In particular, it is noted that the watermarked image is magnified a hundred times.

4.2. Robustness of the Proposed Algorithm. Robustness is a default measure which is used to evaluate the watermarked image's resistance against attacks. In a satisfactory algorithm for image watermark, the watermark would not be easily

TABLE 1: The experimental results of invisibility.

	Lena	Boat	Barbara
The test images			
The watermarked images			
PSNR/MSE	53.1768/0.3129	53.5148/0.2895	53.6411/0.2812
The absolute difference between original images and their corresponding watermarked image			
The extracted watermark			
NC	0.9849	0.9848	0.9850

removed from the watermarked image after common and deliberate attacks. In this paper, we simulate the real situation of disguised attacks and check out robustness for the proposed algorithm, where the number of orientations is 9 and the embedding strength is 0.1.

4.2.1. Robustness to Scaling Attack. For the "Lena" image and "Barbara" image, when scaling parameters are 1/2, 3/4, 3/2, 2, and 4, the extracted watermarks are still distinguishable and NC values are all above 0.90. For the "Boat" image, the extracted watermarks are still distinguishable and NC values are all above 0.90 when scaling parameters are 3/4, 3/2, 2, and 4. With the increase of scaling attack parameter, PSNR values are increasing; MSE values are decreasing. Therefore, the proposed algorithm can resist scaling attack.

4.2.2. Robustness to JPEG Compression Attack. JPEG lossy compression is the most common attack during the transformation of the watermarked image. In order to evaluate robustness of proposed algorithm, every watermarked image is compressed using JPEG with different quality factors. From extracted watermarks in Table 3, it is not hard for anyone to observe that extracted watermark is still distinguishable until the quality factor is set to 30. In addition, for all test images, PSNR values are all above 30 dB; NC values are all above 0.8. Therefore, the proposed algorithm is very robust against JPEG compression.

4.2.3. Robustness to Filtering Attack. As shown in Table 4, whether Gaussian low-pass filtering, average filtering, or median filtering, the extracted watermarks are still distinguishable for the "Lena" image and the "Barbara" image. In addition, NC values are all above 0.855 for the "Lena" image, 0.77 for the "Boat" image, and 0.86 for the "Barbara" image. However, the extracted watermarks are imperfect for the "Boat" image.

4.2.4. Robustness under Various Noises Attack. The watermarked image is easily disturbed by various noises. In the test, we add "Salt and Pepper" (Table 5) noise and "Gaussian" white noise (Table 6) to the watermarked images.

For the watermarked image with "Salt and Pepper" noise, with the increase of noise attack strength, more and more noise points appear in the extracted watermark, but the extracted watermark is still distinguishable and complete until the attack strength is set to 0.05. When the attack strength is set to 0.05, the extracted watermark is not perfect but distinguishable; the NC value is 0.8262 for the Lena image, 0.7866 for the Boat image, and 0.7861 for the Barbara image, respectively.

Similarly, for the watermarked image under the attack of "Gaussian" white noise, when the noise mean is set to zero, noise points increasingly appear in extracted watermark with the increase of noise variance. The extracted watermarks are

TABLE 2: Experimental results under the scaling attack.

Scaling parameter	1/4	1/2	3/4	3/2	2	4
Lena						
PSNR	28.9888	34.6526	40.2526	45.8866	45.7492	45.9472
MSE	82.0732	22.2750	6.1350	1.6766	1.7304	1.6533
NC	0.7778	0.9302	0.9731	0.9824	0.9819	0.9819
The extracted watermark						
Boat						
PSNR	26.3117	31.1662	35.9492	42.4460	42.2792	42.5013
MSE	152.0217	49.7120	16.5257	3.7024	3.8473	3.6540
NC	0.6982	0.8154	0.9009	0.9771	0.9692	0.9712
The extracted watermark						
Barbara						
PSNR	23.6562	25.4999	29.1969	35.8845	35.6902	35.9257
MSE	280.1925	183.2677	78.2331	16.7738	17.5412	16.6155
NC	0.7671	0.9009	0.9658	0.9756	0.9751	0.9751
The extracted watermark						

TABLE 3: Experimental results under the attack of JPEG lossy Compression.
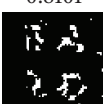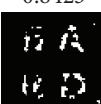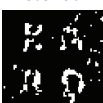
Quality factor	30	40	50	60	75	90
Lena						
PSNR	35.1718	36.0294	36.4005	42.2603	53.2168	48.0330
MSE	19.7649	16.0294	14.8947	6.1242	0.3100	0.8313
NC	0.8252	0.8506	0.9004	0.9160	0.9453	0.9849
The extracted watermark						
Boat						
PSNR	33.3926	34.3324	34.6845	38.6331	53.5308	47.9809
MSE	29.7727	23.9794	22.1121	8.9077	0.2884	1.0351
NC	0.8101	0.8423	0.8955	0.9077	0.9233	0.9834
The extracted watermark						
Barbara						
PSNR	30.6849	31.9392	32.2378	36.1950	53.8219	46.1332
MSE	55.5383	41.6065	38.8416	15.6165	0.2697	1.5840
NC	0.8257	0.8457	0.8706	0.9146	0.9438	0.9834
The extracted watermark						

TABLE 4: Experimental results under filtering attack.
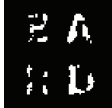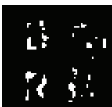
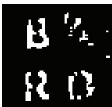| Filter	Gaussian low-pass filtering (13 * 13)	Average filtering (4 * 4)	Average filtering (8 * 8)	Median filtering (3 * 3)	Windows median filtering (2 * 3)	Windows median filtering (3 * 4)
Lena						
PSNR	41.2527	33.8154	31.2694	36.0472	33.0632	30.7585
MSE	4.8731	27.0112	48.5448	16.1570	33.5627	54.7312
NC	0.9619	0.9058	0.8560	0.8955	0.8652	0.8608
The extracted watermark						
Boat						
PSNR	38.8456	31.3718	28.6105	32.1768	29.8478	28.7947
MSE	8.4824	47.4128	89.5425	39.3914	67.3442	85.8246
NC	0.8677	0.7930	0.7710	0.8193	0.7891	0.7764
The extracted watermark						
Barbara						
PSNR	33.7961	25.9565	24.0378	25.3074	24.8688	23.6426
MSE	27.1314	164.9810	256.6278	191.5741	211.9325	281.0734
NC	0.9580	0.8960	0.8604	0.9038	0.8652	0.8901
The extracted watermark						

TABLE 5: Experimental results under the attack of "Salt and Pepper" noise.
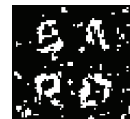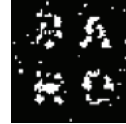
Attack strength	$d = 0.001$	$d = 0.005$	$d = 0.01$	$d = 0.02$	$d = 0.05$
Lena					
PSNR	34.8891	28.3823	25.3281	22.3135	18.4735
MSE	21.0945	94.3727	195.0891	381.7102	924.1257
NC	0.9814	0.9741	0.9741	0.9268	0.8262
The extracted watermark					
Boat					
PSNR	35.5080	28.3722	25.3806	22.4128	18.3500
MSE	18.2927	94.5926	188.3749	373.0794	950.7809
NC	0.9834	0.9712	0.9482	0.9331	0.7866
The extracted watermark					
Barbara					
PSNR	35.3764	28.0243	25.2388	22.5369	18.4612
MSE	18.8555	102.4817	194.6269	362.5728	926.4612
NC	0.9814	0.9717	0.9727	0.9316	0.7861
The extracted watermark					

TABLE 6: Experimental results under the attack of "Gaussian" white noise (mean = 0).

Variance	$v = 0.00001$	$v = 0.00005$	$v = 0.0001$	$v = 0.0005$	$v = 0.001$
Lena					
PSNR	47.9293	42.5216	39.7561	32.9411	29.9570
MSE	1.0475	3.6585	6.8782	33.0349	65.6718
NC	0.9849	0.9766	0.9575	0.8721	0.8345
The extracted watermark					
Boat					
PSNR	48.0248	42.5474	39.7670	32.9706	29.9739
MSE	1.0247	3.6169	6.8608	32.8114	65.4169
NC	0.9854	0.9697	0.9565	0.8643	0.8179
The extracted watermark					
Barbara					
PSNR	48.0677	42.5511	39.7595	32.9428	29.9936
MSE	1.0146	3.6138	6.8727	33.0220	65.1206
NC	0.9844	0.9663	0.9443	0.8701	0.8301
The extracted watermark					

still distinguishable and perfect for all test images until the noise variance is set to 0.0005. When the noise variance is set to 0.0005 and 0.001, the extracted watermark is incomplete but distinguishable for all test images; the NC values are all above 0.8. Therefore, the proposed algorithm can resist noise attack to some extent.

4.2.5. The Comparison Experiments of Related Algorithm. To verify the effectiveness of the proposed algorithm, the proposed algorithm is compared with related algorithms based on DWT and DCT. DCT-based watermark algorithm is performed by embedding watermark in the largest $n \times n$ coefficients of the first-level DCT subband. Watermarking based on DWT is performed by embedding watermark in the largest $n \times n$ coefficients of the first-level subband, where a one-level DWT decomposition is performed using "Haar" wavelet.

To be fair, both the watermark image and the test images are the same to all algorithms. Table 7 shows the results of comparison on "Lena" image. As shown in Table 7, the proposed algorithm outperforms other algorithms in invisibility. Meanwhile, in robustness against these attacks, such as scaling attack and cropping attack, the proposed algorithm gets advantage over other algorithms.

In Table 2, although the NC values of proposed algorithm are not higher than other algorithms except no attack and

scaling attack, it is noted that PSNR values of proposed algorithm are higher than other algorithms except cropping middle (50%). In other words, watermark which is embedded in host image cause much degradation of perceptual quality of the watermarked image, yet the quality of the watermarked image for proposed algorithm is better.

5. Conclusion

This paper tries to implement an image watermark by taking advantage of the unique advantages of extended discrete shearlet and selecting watermark embedding location based on the highest information entropy. The unique advantages of extended discrete shearlet made the watermark system more invisible. Experimental results demonstrate that visual performance of the watermarked images is preferable to that of related algorithms based on DWT and DCT; meanwhile, the proposed watermark algorithm can resist common attack. Therefore, the extended discrete shearlet can be considered as an appropriate transform for digital watermark.

Conflict of Interests

The authors declare that there is no conflict of interests regarding the publication of this paper.

TABLE 7: Comparison on "Lena" image (NC/PSNR).

	DCT	DWT	DST
No attack	0.9849/34.7284 dB	0.9849/33.7641 dB	0.9849/53.1768 dB
Scaling (25%)	0.7699/27.8846 dB	0.7686/28.0819 dB	0.7778/29.9888 dB
Scaling (50%)	0.9243/31.6796 dB	0.9261/31.6349 dB	0.9302/34.6526 dB
Scaling (4)	0.9809/34.7284 dB	0.9749/33.8214 dB	0.9819/45.9472 dB
JPEG (10)	0.8428/29.2431 dB	0.9824/29.0396 dB	0.7056/30.6196 dB
JPEG (30)	0.9429/31.9655 dB	0.9844/31.5159 dB	0.8252/35.1718 dB
JPEG (50)	0.9819/32.5494 dB	0.9849/32.0032 dB	0.9004/36.4005 dB
Cropping right (50%)	0.7222/9.6540 dB	0.9790/9.6459 dB	0.9712/9.6617 dB
Cropping right (75%)	0.7280/7.0743 dB	0.8530/7.0719 dB	0.8579/7.0764 dB
Cropping middle (50%)	0.7100/11.6153 dB	0.8750/27.3320 dB	0.8901/11.6305 dB
Salt & Pepper noise (0.1)	0.6934/15.4339 dB	0.6331/15.3887 dB	0.6729/15.4918 dB

Acknowledgments

References

[1] G. Y. Liu, H. J. Liu, and A. Kadir, "Wavelet-based color pathological image watermark through dynamically adjusting the embedding intensity," *Computational and Mathematical Methods in Medicine*, vol. 2012, Article ID 406349, 10 pages, 2012.

[2] G. Bhatnagar, Q. M. J. Wu, and P. K. Atrey, "Secure randomized image watermarking based on singular value decomposition," *ACM Transactions on Multimedia Computing, Communications and Applications*, vol. 10, no. 1, article 4, 2013.

[3] Y. X. Ma, J. C. Xie, and J. G. Luo, "Image enhancement based on nonsubsampled contourlet transform," in *Proceedings of the 5th International Conference on Information Assurance and Security (IAS '09)*, pp. 31–34, September 2009.

[4] H. Sadreazami and M. Amini, "A robust spread spectrum based image watermarking in ridgelet domain," *AEU—International Journal of Electronics and Communications*, vol. 66, no. 5, pp. 364–371, 2012.

[5] P. Mangaiyarkarasi and S. Arulselvi, "A new digital image watermarking based on finite ridgelet transform and extraction using lCA," in *Proceedings of the International Conference on Emerging Trends in Electrical and Computer Technology*, pp. 837–841, March 2011.

[6] G. Easley, D. Labate, and W.-Q. Lim, "Sparse directional image representations using the discrete shearlet transform," *Applied and Computational Harmonic Analysis*, vol. 25, no. 1, pp. 25–46, 2008.

[7] V. M. Patel, G. R. Easley, and J. Healy, "Shearlet-based deconvolution," *IEEE Transactions on Image Processing*, vol. 18, no. 12, pp. 2673–2685, 2009.

[8] S. Ranjbar, F. Zargari, and M. Ghanbari, "A highly robust two-stage Contourlet-based digital image watermarking method," *Signal Processing: Image Communication*, vol. 28, no. 10, pp. 1526–1536, 2013.

[9] W.-Q. Lim, "The discrete shearlet transform: a new directional transform and compactly supported shearlet frames," *IEEE Transactions on Image Processing*, vol. 19, no. 5, pp. 1166–1180, 2010.

[10] R. Gomathi and A. V. A. Kumar, "An efficient GEM model for image inpainting using a new directional sparse representation: Discrete Shearlet Transform," in *Proceedings of the IEEE International Conference on Computational Intelligence and Computing Research (ICCIC '10)*, pp. 1–4, Coimbatore, India, December 2010.

[11] X.-Y. Wang, Y.-C. Liu, and H.-Y. Yang, "An efficient remote sensing image denoising method in extended discrete shearlet domain," *Journal of Mathematical Imaging and Vision*, vol. 49, no. 2, pp. 434–453, 2014.

[12] C. E. Shanonn and W. Weaver, *The Mathematical Theory of Communication*, University of Illinois Press, 1946.

[13] C. E. Shannon and E. Claude, "A mathematical theory of communication," *Bell System Technical Journal*, vol. 27, no. 3, pp. 379–423, 623–656, 1948.

[14] K. Guo and D. Labate, "Optimally sparse multidimensional representation using shearlets," *SIAM Journal on Mathematical Analysis*, vol. 39, no. 1, pp. 298–318, 2007.